Supercapacitors Hot Paper

Deutsche Ausgabe: DOI: 10.1002/ange.201411533
Internationale Ausgabe: DOI: 10.1002/anie.201411533

Hybrid Fibers Made of Molybdenum Disulfide, Reduced Graphene Oxide, and Multi-Walled Carbon Nanotubes for Solid-State, Flexible, Asymmetric Supercapacitors**

Gengzhi Sun, Xiao Zhang, Rongzhou Lin, Jian Yang, Hua Zhang, and Peng Chen**

Abstract: *One of challenges existing in fiber-based supercapacitors is how to achieve high energy density without compromising their rate stability. Owing to their unique physical, electronic, and electrochemical properties, two-dimensional (2D) nanomaterials, e.g., molybdenum disulfide (MoS_2) and graphene, have attracted increasing research interest and been utilized as electrode materials in energy-related applications. Herein, by incorporating MoS_2 and reduced graphene oxide (rGO) nanosheets into a well-aligned multi-walled carbon nanotube (MWCNT) sheet followed by twisting, MoS_2-rGO/MWCNT and rGO/MWCNT fibers are fabricated, which can be used as the anode and cathode, respectively, for solid-state, flexible, asymmetric supercapacitors. This fiber-based asymmetric supercapacitor can operate in a wide potential window of 1.4 V with high Coulombic efficiency, good rate and cycling stability, and improved energy density.*

As a promising energy-storage device for smart textiles and wearable electronics, fiber-based supercapacitors have attracted much attention in recent years.[1] A number of fiber-based materials have been used in supercapacitors,[2] in which multi-walled carbon nanotube (MWCNT) fibers spun from vertically aligned MWCNT arrays are particularly desirable because of their excellent flexibility, mechanical strength, and electrical conductivity.[3] Although MWCNT fiber-based supercapacitors have been demonstrated,[4] the challenge to improve the energy density still remains. Based on the equation $E = {}^1/_2 CV^2$, where E, C, and V are energy density, specific capacitance, and cell voltage, respectively, E can be improved either by increasing the specific capacitance of the electrode materials or widening the operational voltage range.[5] In addition, the specific capacitance can be enhanced by the incorporation of electrochemically active nanomaterials (e.g., metal oxides or polymers) into MWCNT fibers.[6] However, insufficient attention has been paid to increasing the voltage range, which can be achieved through rational design by combining two materials with different potential windows in the same electrolyte.

Owing to their unique electrochemical properties, two-dimensional (2D) nanosheets of transition-metal dichalcogenides (TMDs, particularly MoS_2),[7] when coupled with conducting materials, have been shown to be promising for various applications, such as hydrogen evolution,[8] lithium-ion batteries,[9] solar cells,[10] and supercapacitors.[11] For example, MoS_2 can efficiently store charges by pseudocapacitance within a positive potential window as a result of the faradaic charge-transfer process on the Mo center (slower process) or the formation of a double-layer at the electrode/electrolyte interface because of the adsorption of protons or other cations on the MoS_2 nanosheet (faster process).[12] This makes MoS_2 an attractive anode material for asymmetric supercapacitors. Herein, for the first time, we incorporate MoS_2 and reduced graphene oxide (rGO) nanosheets into MWCNT fibers to fabricate solid-state, asymmetric supercapacitors by using MoS_2-rGO/MWCNT and rGO/MWCNT fibers as the anode and cathode, respectively. The resulting supercapacitor is extremely flexible and can operate in a wide potential window of 1.4 V with high Coulombic efficiency, good rate and cycling stability, and improved energy density.

In a typical experiment, the continuous MWCNT sheet was pulled out from the vertically aligned MWCNT array grown by chemical-vapor deposition[13] (Figure S1 in the Supporting Information). As schematically shown in Figure 1 a, three layers of MWCNT sheets (width of ca. 1 mm and length of ca. 12 cm) were stacked and then laid on a polytetrafluoroethylene (PTFE) substrate. 2D nanomaterials, such as single-layer MoS_2[14] or GO nanosheets[15] dispersed in DMF, can be introduced into the stacked MWCNT sheet by drop-casting with a pipette, which moved along the MWCNT sheet. The desired amount of each nanomaterial can be tuned by repeating the casting process. The resulting hybrid sheet

[*] Dr. G. Sun,[+] Prof. P. Chen
School of Chemical and Biomedical Engineering
Nanyang Technological University
70 Nanyang Drive, Singapore 637457 (Singapore)
E-mail: ChenPeng@ntu.edu.sg
X. Zhang,[+] J. Yang, Prof. H. Zhang
School of Materials Science and Engineering
Nanyang Technological University
50 Nanyang Avenue, Singapore 639798 (Singapore)
E-mail: HZhang@ntu.edu.sg
Homepage: http://www.ntu.edu.sg/home/hzhang/
R. Lin
School of Mechanical and Aerospace Engineering, Nanyang Technological University
50 Nanyang Avenue, Singapore 639798 (Singapore)
[+] These authors contributed equally to this work.

[**] This work was supported by MOE under AcRF Tier 2 (MOE2014-T2-1-003, MOE2011-T2-2-010, MOE2013-T2-1-034), AcRF Tier 1 (RG 61/12, RGT18/13, and RG5/13), Start-Up Grant (M4080865.070.706022), and the National Research Foundation in Singapore. This Research is also conducted by NTU-HUJ-BGU Nanomaterials for Energy and Water Management Programme under the Campus for Research Excellence and Technological Enterprise (CREATE), that is supported by the National Research Foundation, Prime Minister's Office, Singapore.

Supporting information for this article is available on the WWW under http://dx.doi.org/10.1002/anie.201411533.

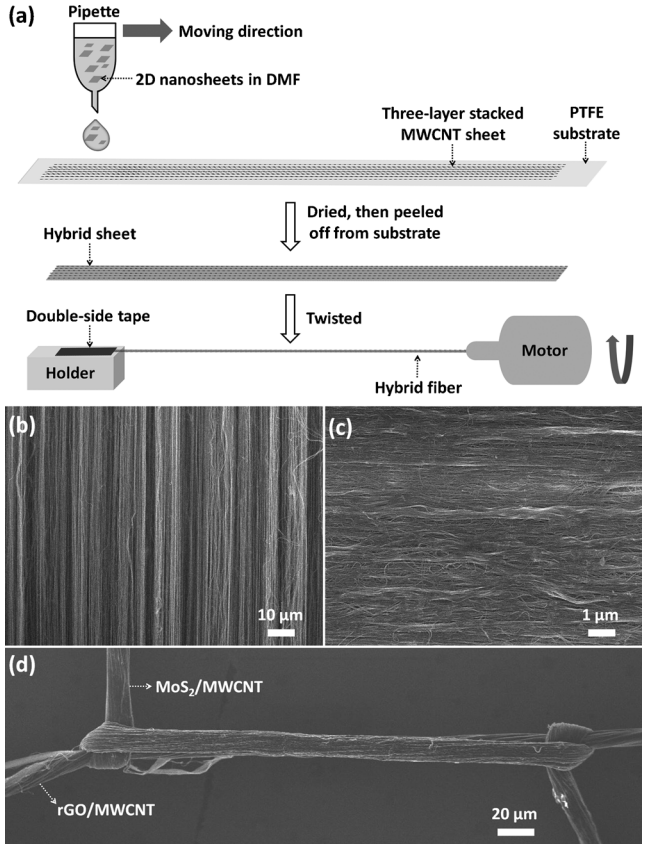

Figure 1. a) Schematic illustration of fabrication of the hybrid fiber. SEM images of b) well-aligned MWCNT sheet, c) MWCNT sheet incorporating MoS_2 nanosheets, and d) tightly knotted MoS_2/MWCNT and rGO/MWCNT fibers.

was dried in vacuum, and then peeled off the PTFE substrate. By using the scotch tape, one end of hybrid sheet was fixed on a glass holder and the other end was fixed to an electric motor, which twisted the sheet at a rotating speed of 200 rpm for 3 min to obtain the hybrid fiber. After the GO/MWCNT fiber was obtained, it was reduced by hydroiodic acid (HI) to give the rGO/MWCNT fiber. The reduction of GO was confirmed by Fourier transform infrared (FT-IR) spectra (Figure S2a), in which the intensity of the bands for the carboxy (3211 cm^{-1}), carbonyl (1716 cm^{-1}), and epoxy (1048 cm^{-1}) groups was greatly decreased. The interlayer distance of rGO calculated based on the X-ray diffraction (XRD) pattern (Figure S2b) was 0.375 nm ($2\theta = 23.7°$), which is less than those of GO (0.762 nm; $2\theta = 11.6°$), further indicative of the removal of oxygen-containing groups on GO.[16]

The nearly perfect alignment of individual MWCNTs in the sheet (Figure 1b) guaranteed the good mechanical strength and electrical conductivity of the MWCNT fibers obtained by twisting.[17] Figure 1c shows a typical SEM image of a hybrid MWCNT sheet incorporating MoS_2 nanosheets. The incorporation of MoS_2 in the resultant MoS_2/MWCNT hybrid fiber was confirmed by the energy-dispersive X-ray spectroscopy (EDS; Figure S3). In our experiments, the hybrid fibers retain excellent flexibility after the incorporation of 2D nanomaterials (MoS_2 and rGO) and can be tightly knotted (Figure 1d). The conductivity of bare MWCNT fiber is approximately 300 $S\,cm^{-1}$, which decreases with an increasing amount of 2D nanosheets (Figure S4).

As a proof-of-concept application, the capacitive performance of the MoS_2/MWCNT fiber was investigated in a two-electrode configuration at a charge–discharge current of 1 μA (0.13 $A\,cm^{-3}$). Polyvinyl alcohol (PVA)-H_2SO_4 gel was used as the solid-state electrolyte. The specific volumetric capacitance (C_V) was calculated from the discharge curve and normalized to the volume of the electrodes. As expected, C_V improved after the addition of MoS_2 in a dose-dependent manner (Figure S5). However, the improvement is moderate, possibly because of the non-ideal coupling between the 2D MoS_2 nanosheets and the 1D MWCNT.

We speculated that 2D rGO nanosheets, which can intimately interact with both MoS_2[18] and MWCNTs,[19] may mediate the coupling between the electrochemically active MoS_2 nanosheets and the conductive MWCNTs. In a typical experiment, the mixture of GO and MoS_2 in DMF was drop-cast onto a MWCNT sheet to fabricate MoS_2-GO/MWCNT hybrid fiber. GO nanosheets can assist the dispersion of MoS_2 nanosheets and later incorporation into the MWCNT sheet. After the chemical reduction of the MoS_2-GO/MWCNT hybrid fiber with HI, the MoS_2-rGO/MWCNT fiber was obtained. The weight ratio between GO and MWCNT is kept at 3:7 because a too low amount of rGO cannot effectively improve the capacitive performance of hybrid fibers,[18b] while too large an amount of rGO can significantly compromise the fiber conductivity (Figure S4).

The resultant MoS_2-rGO/MWCNT fiber-based supercapacitors with various amounts of MoS_2 were tested using cyclic voltammetry (CV) and galvanostatic charge–discharge measurements. As shown in Figure 2a, CV curves measured at 100 $mV\,s^{-1}$ are nearly rectangular, indicating the high electrical conductivity of well-aligned fibers. The maximum current density was obtained at 6.3 wt% of MoS_2. The specific capacitances were calculated based on the galvanostatic charge–discharge curves at current of 2 μA or 0.5 $A\,cm^{-3}$ (Figure 2b). The C_V of MoS_2-rGO/MWCNT fiber-based supercapacitor reached the maximum value of 4.8 $F\,cm^{-3}$ at 6.3 wt% of MoS_2, which is significantly improved as compared to the devices made of MoS_2/MWCNT, rGO/MWCNT (i.e. 0 wt% of MoS_2 in MoS_2-rGO/MWCNT) or bare MWCNT fibers (Figure 2b). Figure 2c depicts the galvanostatic charge–discharge curves of MoS_2-rGO/MWCNT (6.3 wt% of MoS_2) fiber-based supercapacitors at charge-discharge current densities ranging from 0.07 to 2 $A\,cm^{-3}$. In our experiment, C_V decreased to 3.8 $F\,cm^{-3}$ at the high current density, 2.0 $A\,cm^{-3}$ (Figure 2d).

To estimate the potential windows of MoS_2-rGO/MWCNT and rGO/MWCNT hybrid fiber electrodes, CV measurements were conducted in 1 M H_2SO_4 solution using the three-electrode configuration, in which Pt foil and Ag/AgCl wire in saturated KCl solution were used as the counter electrode and reference electrode, respectively. As shown in Figure 3a, when the voltage was higher than 0.8 V or lower than −0.6 V, the oxidation and reduction current increased in the MoS_2-rGO/MWCNT and rGO/MWCNT electrodes, respectively. It suggests that an asymmetric supercapacitor

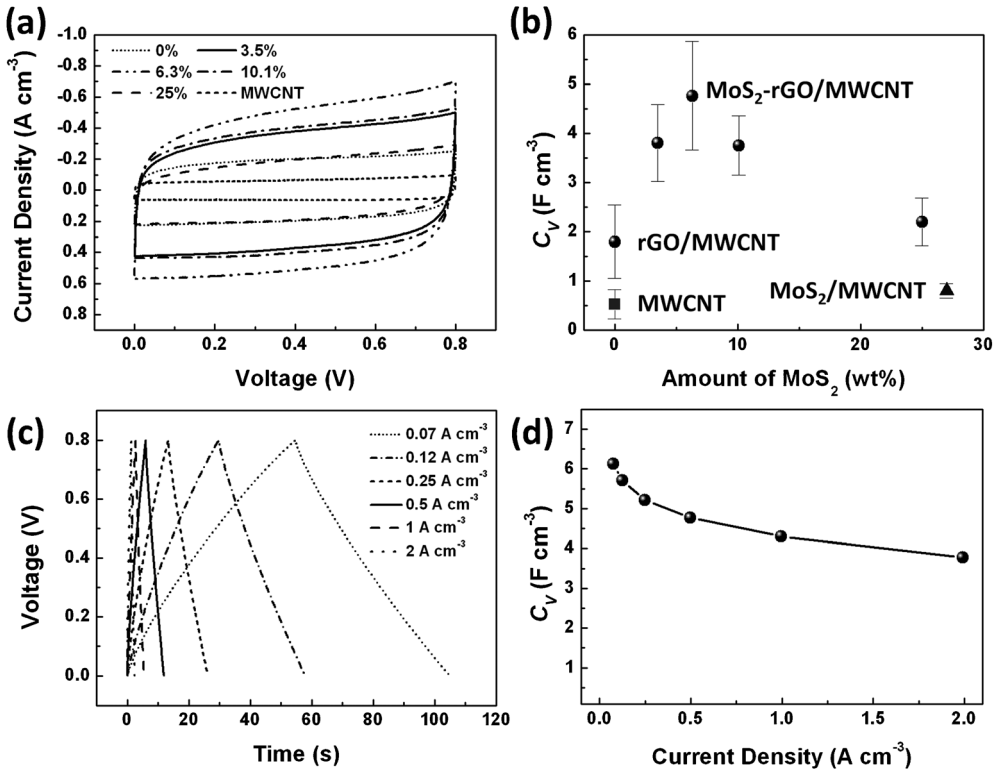

Figure 2. a) CV curves of MoS_2-rGO/MWCNT fiber-based supercapacitors with varying amount of MoS_2 (0, 3.5, 6.3, 10.1, and 25 wt%). b) Volumetric capacitance (C_V) of MoS_2-rGO/MWCNT fiber-based supercapacitors as a function of the amount (wt%) of MoS_2 (dots), bare MWCNT fiber (square), and MoS_2/MWCNT fiber (27 wt% of MoS_2, triangle). c) Galvanostatic charge–discharge curves of MoS_2-rGO/MWCNT fiber-based supercapacitor at current densities of 0.07, 0.12, 0.25, 0.5, 1, and 2 A cm^{-3}. d) Current density dependent C_V of MoS_2-rGO/MWCNT fiber-based supercapacitor.

using MoS_2-rGO/MWCNT as anode and rGO/MWCNT as cathode has a stable potential window of 1.4 V.

The asymmetric device was fabricated by placing MoS_2-rGO/MWCNT and rGO/MWCNT fibers in parallel on a substrate, such as glass slide or polyethylene terephthalate (PET) film, with gap of approximately 0.5 mm. PVA-H_2SO_4 gel was then coated on the fibers as the solid-state electrolyte (inset of Figure 3b). Ag paste was applied at both ends for electrochemical measurements. The asymmetric supercapacitor can be cycled reversibly with a cell voltage up to 1.4 V, while the oxidation current becomes noticeable at 1.6 V (Figure 3b). As expected, the C_V increased with the voltage, whereas the Coulombic efficiency decreased (Figure 3c). The sharp drop of Coulombic efficiency beyond 1.4 V may be attributed to a redox reaction, such as oxidation of MoS_2 or evolution of H_2.[18b,20] In the following experiment, the cell voltage was fixed at 1.4 V. The C_V of fiber-based asymmetric supercapacitor calculated based on the charge–discharge curves (Figure 3d) is 5.2 F cm^{-3} at current density of 0.16 A cm^{-3} (Figure 3e). The voltage drop (*IR* drop) at the initial of discharging process is attributable to the internal resistance of the supercapacitor, which is a good evaluation for rate stability.[21] Normally, good rate stability requires a small *IR* drop. As shown in Figure 3e, the *IR* drop is negligible at low current density, while at high current density of 3.3 A cm^{-3}, it remains as small as around 0.1 V which is similar to the value obtained in the bare MWCNT fiber-based symmetric supercapacitor.[22] As a result, when compared to the previously reported fiber-based symmetric supercapacitors with MWCNT fibers, rGO fibers or rGO/CNT fibers,[2d,4b,22,23] the C_V obtained here is much more stable at high current densities (61% retention at the current density as high as 3.3 A cm^{-3}).

The energy density and power density can be calculated by $E = {}^1/_2 C V^2$ and $P = E/t_{discharge}$, respectively, where C, V, and $t_{discharge}$ are the capacitance, voltage range, and discharging time, respectively. E and P depend on the electrode conductivity, diffusion kinetics of electrolytes, and electrochemical kinetics of MoS_2. Compared to the symmetric devices, supercapacitors with asymmetric design can use two electrodes with different potential windows to increase the cell voltage and specific capacitance. As a result, at a given P, the E of the fiber-based asymmetric device (inset of Figure 3b) is significantly enhanced without compromising power density, and superior to the symmetric devices made of MoS_2-rGO/MWCNT, rGO/MWCNT, and bare MWCNT fibers (inset of Figure 3f). In addition, the performance of our asymmetric supercapacitor is better than that of fiber-based supercapacitors consisting of MnO_2/carbon fibers,[24] MWCNT fibers,[22] and carbon fibers coated by MnO_2/ZnO,[25] and comparable to that of fiber-based supercapacitors based on carbonaceous fibers[26] and PEDOT/MWCNT fibers[6b] (Figure 3f). As seen from Figure 4a, the CV curve of the fiber-based asymmetric device on PET does not alter even if the device was bent through 180°, that is, completely folded, which demonstrates the excellent flexibility of the device. Furthermore, both C_V and Coulombic efficiency are steady with or without bending even after 7000 cycles, indicating the high robustness of the device.

In summary, flexible hybrid fibers were fabricated by incorporation of 2D MoS_2 and rGO nanosheets into well-aligned MWCNT sheets followed by twisting. A solid-state, fiber-based asymmetric supercapacitor was then fabricated by using the fabricated MoS_2-rGO/MWCNT and rGO/MWCNT fibers as the anode and cathode, respectively. This fiber-based asymmetric device showed high energy density, good rate and cycling stability owing to the wide potential window, electro-

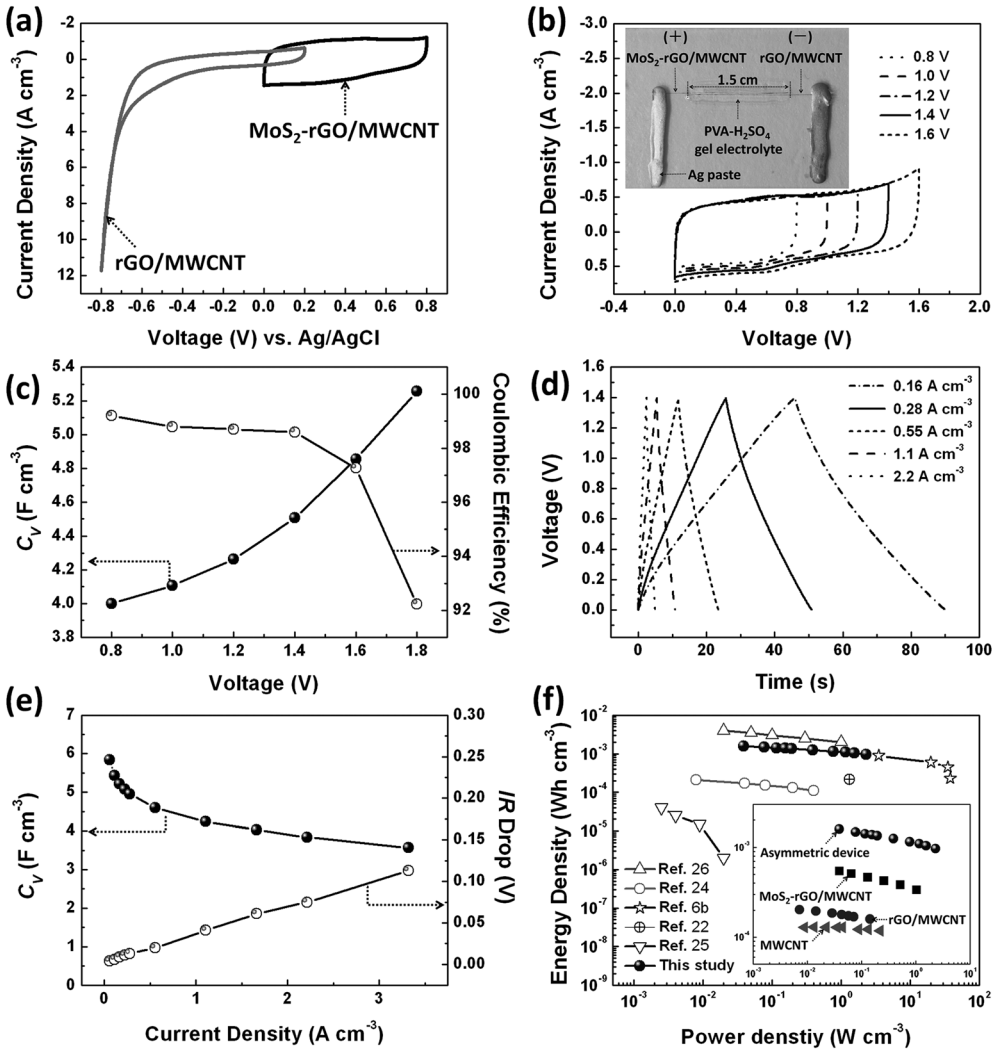

Figure 3. a) CV curves of rGO/MWCNT fiber and MoS_2-rGO/MWCNT fiber in three-electrode system. b) CV curves of the fiber-based asymmetric supercapacitor at cell voltage of 0.8, 1, 1.2, 1.4, and 1.6 V. Inset: Optical image of a fiber-based asymmetric supercapacitor on glass slide. c) Volumetric capacitance (C_V) and Coulombic efficiency of the fiber-based asymmetric supercapacitor as the function of cell voltage. d) Galvanostatic charge–discharge curves of the fiber-based asymmetric supercapacitor at current density of 0.16, 0.28, 0.55, 1.1 and 2.2 A cm^{-3}. e) C_V and *IR* drop of the fiber-based asymmetric supercapacitor as a function of current density. f) Plot of energy density versus power density for our fiber-based asymmetric supercapacitor and other reported fiber-based supercapacitors. Inset: plot of energy density versus power density for our fiber-based asymmetric supercapacitor and those of MoS_2-rGO/MWCNT, rGO/MWCNT, and bare MWCNT fiber-based symmetric supercapacitors.

chemical activity of MoS_2, electrical conductivity of well-aligned MWCNT fiber, and the incorporation of rGO. This kind of fiber-based asymmetric devices might have promising applications in flexible electronics.

Experimental Section

As described previously,[13a–c] the vertically aligned multi-walled carbon nanotube (MWCNT) array was prepared by chemical vapor deposition (CVD) in a quartz tube furnace using a thin Fe film (1 nm) deposited on Si/SiO_2 substrate as catalyst, and Ar (155 sccm) and C_2H_4 (45 sccm) as the carrier gas and carbon source, respectively. The growth of MWCNT array was carried out at 750 °C for 10 min. The well-aligned MWCNT sheet pulled from the array has a density of 2.12 μg cm^{-2} (one layer), which was measured using a microbalance (METTLER TOLEDO, M × 5) with a readability of 1 μg. Graphene oxide (GO) was prepared by a modified Hummer method,[27] and then dispersed in dimethylformamide (DMF, 99.8%, anhydrous, Sigma–Aldrich) with concentration of 1 and 5 mg mL^{-1}. The single-layer molybdenum disulfide (MoS_2) nanosheets were prepared by the electrochemical intercalation method as reported by our previous study.[14] After the exfoliation, the as-prepared single-layer MoS_2 nanosheets were re-dispersed in DMF with concentration of ca. 0.8 mg mL^{-1} and ultrasonicated prior to use.

Three-layers of MWCNT sheets (width of ca. 1 mm and length of ca. 12 cm) were stacked and then laid on a polytetrafluoroethylene (PTFE) substrate. Single-layer MoS_2, GO, and the mixture of MoS_2 and GO nanosheets were introduced into MWCNT sheet by drop-casting. The amount of each material can be tuned by repeating the casting process. The resulting hybrid sheet was dried in vacuum, then peeled off from the PTFE substrate and further twisted into fibers with a motor (200 rpm for 3 min). The obtained GO/MWCNT and MoS_2-GO/MWCNT fibers were immersed into hydroiodic acid (HI (55 wt%), Sigma Aldrich, ACS reagent) at room temperature for 12 h to reduce GO and obtain rGO.[28]

The inset of Figure 3b showed an optical image of the as-fabricated solid-state fiber-based asymmetric supercapacitor. The MoS_2-rGO/MWCNT and rGO/MWCNT fibers were placed closely and in parallel on glass, and then coated with polyvinyl alcohol (PVA, Sigma Aldrich, M_W 85000–124000)-H_2SO_4 gel electrolyte. The PVA-H_2SO_4 gel electrolyte was prepared by mixing H_2SO_4 (aqueous solution of 1 M, 10 mL) with PVA powder (1 g), which was heated at 90 °C with vigorous stirring to obtain a homogeneous gel-like suspension. Ag paste applied at both ends of the fibers served as the electrical pad for electrochemical measurements. The capacitive performance was tested in two-electrode configuration. Polyethylene terephthalate (PET, 0.3 mm thick) film (3 M Company, USA), was used as alternative substrate to test the flexibility of the asymmetric supercapacitors.

The SEM images and EDS were performed on a field-emission scanning electron microscope (JEOL, JSM-6700F, Japan). The

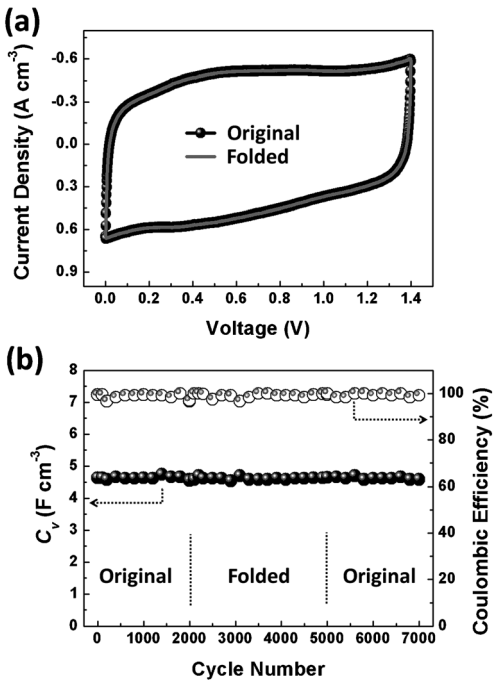

Figure 4. a) CV curves of a fiber-based asymmetric device at original or folded states. b) Cycling and bending stability of volumetric capacitance (C_V) and Coulombic efficiency at current density of 0.55 A cm^{-3}.

electrical properties of hybrid fibers were characterized using Agilent Technologies B1500 A (USA). FT-IR spectra were recorded with a PerkinElmer FT-IR Spectrum GX spectrometer. XRD patterns were recorded with Bruker 6000 X-ray diffractometer using a $Cu_{K\alpha}$ source. The electrochemical measurements were obtained by a CHI 660D electrochemical work station.

The specific volumetric capacitance (C_V) of fiber-based supercapacitor was calculated from the charge-discharge curve according to the following Equation (1):[29]

$$C_V = [i/(dV/dt)]/V_{fiber} \quad (1)$$

where i is the discharging current, dV/dt is the slope of discharge curve, and V_{fiber} refers to the total volume of two fibers.

Keywords: carbon nanotubes · flexible devices · graphene · molybdenum disulfide · supercapacitors

How to cite: *Angew. Chem. Int. Ed.* **2015**, *54*, 4651 – 4656
Angew. Chem. **2015**, *127*, 4734 – 4739

[1] G. Z. Sun, X. W. Wang, P. Chen, *Mater. Today* **2015**, DOI: 10.1016/j.mattod.2014.12.001.

[2] a) Y. P. Fu, X. Cai, H. W. Wu, Z. B. Lv, S. C. Hou, M. Peng, X. Yu, D. C. Zou, *Adv. Mater.* **2012**, *24*, 5713 – 5718; b) J. Bae, M. K. Song, Y. J. Park, J. M. Kim, M. L. Liu, Z. L. Wang, *Angew. Chem. Int. Ed.* **2011**, *50*, 1683 – 1687; *Angew. Chem.* **2011**, *123*, 1721 – 1725; c) V. T. Le, H. Kim, A. Ghosh, J. Kim, J. Chang, Q. A. Vu, D. T. Pham, J. H. Lee, S. W. Kim, Y. H. Lee, *ACS Nano* **2013**, *7*, 5940 – 5947; d) Y. N. Meng, Y. Zhao, C. G. Hu, H. H. Cheng, Y. Hu, Z. P. Zhang, G. Q. Shi, L. T. Qu, *Adv. Mater.* **2013**, *25*, 2326 – 2331; e) Z. B. Yang, J. Deng, X. L. Chen, J. Ren, H. S. Peng, *Angew. Chem. Int. Ed.* **2013**, *52*, 13453 – 13457; *Angew. Chem.* **2013**, *125*, 13695 – 13699.

[3] a) G. Z. Sun, Y. N. Zhang, L. X. Zheng, *J. Nanomater.* **2012**, *2012*, 506209; b) G. Z. Sun, L. X. Zheng, J. Y. Zhou, Y. N. Zhang, Z. Y. Zhan, J. H. L. Pang, *Int. J. Plast.* **2013**, *40*, 56 – 64; c) Y. N. Zhang, L. X. Zheng, G. Z. Sun, Z. Y. Zhan, K. Liao, *Carbon* **2012**, *50*, 2887 – 2893; d) K. L. Jiang, J. P. Wang, Q. Q. Li, L. A. Liu, C. H. Liu, S. S. Fan, *Adv. Mater.* **2011**, *23*, 1154 – 1161.

[4] a) G. Z. Sun, J. Y. Zhou, F. Yu, Y. N. Zhang, J. H. L. Pang, L. X. Zheng, *J. Solid State Electrochem.* **2012**, *16*, 1775 – 1780; b) J. Ren, L. Li, C. Chen, X. L. Chen, Z. B. Cai, L. B. Qiu, Y. G. Wang, X. R. Zhu, H. S. Peng, *Adv. Mater.* **2013**, *25*, 1155 – 1159.

[5] a) J. Chang, M. Jin, F. Yao, T. H. Kim, V. T. Le, H. Yue, F. Gunes, B. Li, A. Ghosh, S. Xie, Y. H. Lee, *Adv. Funct. Mater.* **2013**, *23*, 5074 – 5083; b) Z. J. Fan, J. Yan, T. Wei, L. J. Zhi, G. Q. Ning, T. Y. Li, F. Wei, *Adv. Funct. Mater.* **2011**, *21*, 2366 – 2375.

[6] a) C. Choi, J. A. Lee, A. Y. Choi, Y. T. Kim, X. Lepro, M. D. Lima, R. H. Baughman, S. J. Kim, *Adv. Mater.* **2014**, *26*, 2059 – 2065; b) J. A. Lee, M. K. Shin, S. H. Kim, H. U. Cho, G. M. Spinks, G. G. Wallace, M. D. Lima, X. Lepro, M. E. Kozlov, R. H. Baughman, S. J. Kim, *Nat. Commun.* **2013**, *4*, 1970.

[7] a) X. Huang, C. Tan, Z. Yin, H. Zhang, *Adv. Mater.* **2014**, *26*, 2185 – 2204; b) X. Huang, Z. Y. Zeng, H. Zhang, *Chem. Soc. Rev.* **2013**, *42*, 1934 – 1946; c) C. Tan, H. Zhang, *Chem. Soc. Rev.* **2015**, DOI: 10.1039/c4s00182f.

[8] a) Y. H. Chang, C. T. Lin, T. Y. Chen, C. L. Hsu, Y. H. Lee, W. J. Zhang, K. H. Wei, L. J. Li, *Adv. Mater.* **2013**, *25*, 756 – 760; b) Z. Y. Zeng, C. L. Tan, X. Huang, S. Y. Bao, H. Zhang, *Energy Environ. Sci.* **2014**, *7*, 797 – 803; c) C. B. Ma, X. Y. Qi, B. Chen, S. Y. Bao, Z. Y. Yin, X. J. Wu, Z. M. Luo, J. Wei, H. L. Zhang, H. Zhang, *Nanoscale* **2014**, *6*, 5624 – 5629; d) J. Z. Chen, X. J. Wu, L. S. Yin, B. Li, X. Hong, Z. X. Fan, B. Chen, C. Xue, H. Zhang, *Angew. Chem. Int. Ed.* **2015**, *54*, 1210 – 1214; *Angew. Chem.* **2015**, *127*, 1226 – 1230.

[9] a) T. Stephenson, Z. Li, B. Olsen, D. Mitlin, *Energy Environ. Sci.* **2014**, *7*, 209 – 231; b) C. B. Zhu, X. K. Mu, P. A. van Aken, Y. Yu, J. Maier, *Angew. Chem. Int. Ed.* **2014**, *53*, 2152 – 2156; *Angew. Chem.* **2014**, *126*, 2184 – 2188; c) X. H. Cao, Y. M. Shi, W. H. Shi, X. H. Rui, Q. Y. Yan, J. Kong, H. Zhang, *Small* **2013**, *9*, 3433 – 3438.

[10] X. Gu, W. Cui, H. Li, Z. W. Wu, Z. Y. Zeng, S. T. Lee, H. Zhang, B. Q. Sun, *Adv. Energy Mater.* **2013**, *3*, 1262 – 1268.

[11] L. J. Cao, S. B. Yang, W. Gao, Z. Liu, Y. J. Gong, L. L. Ma, G. Shi, S. D. Lei, Y. H. Zhang, S. T. Zhang, R. Vajtai, P. M. Ajayan, *Small* **2013**, *9*, 2905 – 2910.

[12] a) A. Ramadoss, T. Kim, G. S. Kim, S. J. Kim, *New J. Chem.* **2014**, *38*, 2379 – 2385; b) J. M. Soon, K. P. Loh, *Electrochem. Solid-State Lett.* **2007**, *10*, A250 – A254.

[13] a) L. X. Zheng, G. Z. Sun, Z. Y. Zhan, *Small* **2010**, *6*, 132 – 137; b) G. Z. Sun, J. H. L. Pang, J. Y. Zhou, Y. N. Zhang, Z. Y. Zhan, L. X. Zheng, *Appl. Phys. Lett.* **2012**, *101*, 131905; c) G. Z. Sun, D. Wang, J. H. L. Pang, J. Liu, L. X. Zheng, *Appl. Phys. Lett.* **2013**, *103*, 131902; d) G. Z. Sun, J. Q. Liu, L. X. Zheng, W. Huang, H. Zhang, *Angew. Chem. Int. Ed.* **2013**, *52*, 13351 – 13355; *Angew. Chem.* **2013**, *125*, 13593 – 13597.

[14] Z. Y. Zeng, Z. Y. Yin, X. Huang, H. Li, Q. Y. He, G. Lu, F. Boey, H. Zhang, *Angew. Chem. Int. Ed.* **2011**, *50*, 11093 – 11097; *Angew. Chem.* **2011**, *123*, 11289 – 11293.

[15] X. C. Dong, G. C. Xing, M. B. Chan-Park, W. H. Shi, N. Xiao, J. Wang, Q. Y. Yan, T. C. Sum, W. Huang, P. Chen, *Carbon* **2011**, *49*, 5071 – 5078.

[16] G. Z. Sun, L. X. Zheng, Z. Y. Zhan, J. Y. Zhou, X. B. Liu, L. Li, *Carbon* **2014**, *68*, 748 – 754.

[17] a) G. Z. Sun, L. X. Zheng, J. An, Y. Z. Pan, J. Y. Zhou, Z. Y. Zhan, J. H. L. Pang, C. K. Chua, K. F. Leong, L. Li, *Nanoscale* **2013**, *5*, 2870 – 2874; b) X. M. Sun, T. Chen, Z. B. Yang, H. S. Peng, *Acc. Chem. Res.* **2013**, *46*, 539 – 549.

[18] a) G. Z. Sun, J. Q. Liu, X. Zhang, X. W. Wang, H. Li, Y. Yu, W. Huang, H. Zhang, P. Chen, *Angew. Chem. Int. Ed.* **2014**, *53*, 12576 – 12580; *Angew. Chem.* **2014**, *126*, 12784 – 12788; b) E. G. D. Firmiano, A. C. Rabelo, C. J. Dalmaschio, A. N.

Pinheiro, E. C. Pereira, W. H. Schreiner, E. R. Leite, *Adv. Energy Mater.* **2014**, *4*, 1301380.
[19] H. Sun, X. You, J. E. Deng, X. L. Chen, Z. B. Yang, J. Ren, H. S. Peng, *Adv. Mater.* **2014**, *26*, 2868 – 2873.
[20] A. B. Laursen, S. Kegnaes, S. Dahl, I. Chorkendorff, *Energy Environ. Sci.* **2012**, *5*, 5577 – 5591.
[21] G. M. Wang, H. Y. Wang, X. H. Lu, Y. C. Ling, M. H. Yu, T. Zhai, Y. X. Tong, Y. Li, *Adv. Mater.* **2014**, *26*, 2676 – 2682.
[22] P. Xu, T. L. Gu, Z. Y. Cao, B. Q. Wei, J. Y. Yu, F. X. Li, J. H. Byun, W. N. Lu, Q. W. Li, T. W. Chou, *Adv. Energy Mater.* **2014**, *4*, 1300759.
[23] D. Yu, K. Goh, H. Wang, L. Wei, W. Jiang, Q. Zhang, L. M. Dai, Y. Chen, *Nat. Nanotechnol.* **2014**, *9*, 555 – 562.
[24] X. Xiao, T. Q. Li, P. H. Yang, Y. Gao, H. Y. Jin, W. J. Ni, W. H. Zhan, X. H. Zhang, Y. Z. Cao, J. W. Zhong, L. Gong, W. C. Yen, W. J. Mai, J. Chen, K. F. Huo, Y. L. Chueh, Z. L. Wang, J. Zhou, *ACS Nano* **2012**, *6*, 9200 – 9206.
[25] P. H. Yang, X. Xiao, Y. Z. Li, Y. Ding, P. F. Qiang, X. H. Tan, W. J. Mai, Z. Y. Lin, W. Z. Wu, T. Q. Li, H. Y. Jin, P. Y. Liu, J. Zhou, C. P. Wong, Z. L. Wang, *ACS Nano* **2013**, *7*, 2617 – 2626.
[26] D. S. Yu, K. L. Goh, Q. Zhang, L. Wei, H. Wang, W. C. Jiang, Y. Chen, *Adv. Mater.* **2014**, *26*, 6790 – 6797.
[27] X. Z. Zhou, X. Huang, X. Y. Qi, S. X. Wu, C. Xue, F. Y. C. Boey, Q. Y. Yan, P. Chen, H. Zhang, *J. Phys. Chem. C* **2009**, *113*, 10842 – 10846.
[28] a) S. F. Pei, J. P. Zhao, J. H. Du, W. C. Ren, H. M. Cheng, *Carbon* **2010**, *48*, 4466 – 4474; b) I. K. Moon, J. Lee, R. S. Ruoff, H. Lee, *Nat. Commun.* **2010**, *1*, 73.
[29] M. Stoller, R. S. Ruoff, *Energy Environ. Sci.* **2010**, *3*, 1294 – 1301.

Received: November 29, 2014
Revised: January 4, 2015
Published online: February 18, 2015

